

CONSTRAINTS ON H_0 FROM THE CENTRAL VELOCITY DISPERSIONS OF LENS GALAXIES

Aaron J. Romanowsky and Christopher S. Kochanek

Harvard-Smithsonian Center for Astrophysics, MS-10, 60 Garden Street, Cambridge MA 02138

Email: aromanowsky@cfa.harvard.edu

ABSTRACT

We employ Schwarzschild's method of orbit modeling to constrain the mass profiles of the central lens galaxies in Q0957+561 and PG 1115+080. We combine the measured central projected stellar velocity dispersions of these galaxies with the self-similar radial profiles of the rms velocity and of the Gauss-Hermite moment h_4 observed in nearby galaxies for $0 \lesssim R \lesssim 2R_{\text{eff}}$. For Q0957+561, we find a 16% uncertainty in the galaxy mass, and formal $2\text{-}\sigma$ limits on the Hubble constant of $H_0 = 61^{+13}_{-15} \text{ km s}^{-1} \text{ Mpc}^{-1}$. For PG 1115+080, we find that none of the viable lens models can be ruled out, so that H_0 is not yet strongly constrained by this system.

Subject headings: galaxies: elliptical and lenticular, cD — galaxies: structure — galaxies: fundamental parameters — galaxies: kinematics and dynamics — gravitational lensing — quasars: individual (Q0957+561) — quasars: individual (PG 1115+080) — distance scale — dark matter

1. INTRODUCTION

The gravitational lens system Q0957+561 (Walsh, Carswell, & Weymann 1979) has been modeled extensively in an effort to determine the Hubble constant H_0 from measurements of the time delay between its two primary images. Since the long-running dispute over the time delay measurement has been resolved in favor of the short delay (Schild & Thomson 1997; Haarsma *et al.* 1997, 1998; Kundić *et al.* 1997), the largest remaining uncertainty arises from the mass model. The lens consists of a cluster with a large central elliptical galaxy G1. The asymmetric radial positions of the images accurately constrain the parameterized radial mass distribution of G1 (Grogan & Narayan 1996, hereafter GN). However, the presence of the cluster introduces a degeneracy in the overall mass normalization of G1 (Falco, Gorenstein, & Shapiro 1985; Gorenstein, Falco, & Shapiro 1988), and thus in the determination of the Hubble constant ($H_0 \propto \sigma_0^2$, where σ_0 is a velocity dispersion characterizing the mass of G1). Therefore, additional independent constraints are needed on the relative contributions of G1 and the cluster to the $6''$ image separation. These can be obtained by inferring *the mass of the cluster* from cluster dynamics (Garrett, Walsh, & Carswell 1992; Angonin-Willaime, Soucail, & Vanderriest 1994), from hot intracluster gas X-ray emission

(Chartas *et al.* 1995, 1998), or from the weak lensing of background galaxies (Dahle, Maddox, & Lilje 1994; Fischer *et al.* 1997). Alternatively, one can infer *the mass of G1* from stellar dynamical measurements.

The quadruple lens PG 1115+080 (Weymann *et al.* 1980) is the second system with a well-determined time delay (Schechter *et al.* 1997; Barkana 1997b). The projected mass of the primary lens galaxy G inside the ring of images can be precisely determined (unlike the case of Q0957+561, uncertainties in the mass distribution of nearby galaxies have only a minor effect on the models). However, the geometry of the system does not permit distinguishing between different mass profiles. This has important consequences for the Hubble constant, since H_0 can vary by 40%, depending on the mass model assumed (see Keeton & Kochanek 1997; Courbin *et al.* 1997; Saha & Williams 1997; Impey *et al.* 1998). Stellar dynamical measurements of G may be helpful for breaking the degeneracy in the mass model, and thus in H_0 .

Falco *et al.* (1997) measured the central projected stellar velocity dispersion of Q0957+561 G1 to be $\hat{\sigma}_p = 279 \pm 12 \text{ km s}^{-1}$, improving on an earlier measurement by Rhee (1991). Similarly, Tonry (1998) measured the central dispersion of PG 1115+080 G to be $\hat{\sigma}_p = 281 \pm 25 \text{ km s}^{-1}$. However, the conversion of the measured $\hat{\sigma}_p$ to σ_0 is subject to systematic uncertainties, which include the unknown anisotropy structure of the stellar orbits, the radial variation of the mass-to-light ratio, and the ellipticity of the galaxy. Previous galaxy models have arrived at a relatively small uncertainty in this conversion by making arbitrary simplifying assumptions. Kochanek (1993, 1994) considered a singular isothermal mass model with constant anisotropy. For Q0957+561, GN used these dynamical models, but limited them to be nearly isotropic, leading to a 2% systematic uncertainty in σ_0^2 (and thus in H_0). Barkana (1997a) also assumed near-isotropic orbits, leading to an uncertainty in H_0 of 4%, but he noted that allowing for more anisotropy gives an uncertainty of 14%. In fact, dynamical studies of nearby elliptical galaxies have clearly demonstrated that there is little basis for the assumption of isotropy, or even of constant anisotropy.

Binney & Mamon (1982) and Tonry (1983) first illustrated that an elliptical galaxy’s surface brightness and projected stellar velocity dispersion profiles, $I(R)$ and $\sigma_p(R)$, could not determine both its mass distribution and its anisotropy profile. Richstone & Tremaine (1984) and Katz & Richstone (1985) used orbit modeling methods to demonstrate that the conversion from the dispersion profile $\sigma_p(R)$ to a mass parameter σ_0^2 can be uncertain by an order of magnitude. Further theoretical studies (Dejonghe 1987; Merritt 1987; Merrifield & Kent 1990; Gerhard 1991; Dejonghe & Merritt 1992; Merritt & Saha 1993; Merritt 1993) demonstrated that *complete* knowledge of the stellar line-of-sight velocity distribution (LOSVD) $\mathcal{L}(v_p, R)$ gives a unique solution for the two-integral distribution function (DF) $f(E, L)$ in a known spherical potential Φ , and may even strongly constrain an unknown Φ . The general efficacy of *incomplete* knowledge of \mathcal{L} is less clear, but important constraints on f and Φ could be further provided by large-radius measurements of higher-order velocity moments (*e.g.*, the Gauss-Hermite moments h_l — van der Marel & Franx 1993; Gerhard 1993; see also Rix & White 1992; Zhao & Prada 1996). Rix *et al.* (1997) and Gerhard *et al.* (1998) made dynamical fits to nearby galaxies with higher-order moments (h_3, h_4) measured to $\sim 2.5R_{\text{eff}}$; they determined the total mass to $\sim 10\text{-}15\%$, and ruled out a constant

mass-to-light ratio with $> 99\%$ confidence. For the galaxy NGC 2434, the solutions typically had nearly constant radial anisotropy $\beta(r) \equiv (1 - v_\theta^2/v_r^2) \simeq 0.5$, while NGC 6703 showed an anisotropy rising from $\beta \sim 0.1$ at the center to ~ 0.4 near R_{eff} . *Thus the assumption of $\beta(r) = 0$, or even of constant $\beta(r)$, is certainly unwarranted and probably incorrect.*

While our current knowledge of elliptical galaxies does not permit us to make arbitrary assumptions about the anisotropy of the DF, we can impose the constraint that the unmeasured $\sigma_p(R)$ and $h_4(R)$ profiles of these lens galaxies are similar to those of other galaxies (provided they are universally homologous). In this study we rigorously consider the utility of the central $\hat{\sigma}_p$ measurement for determining H_0 from these two lens systems. To ensure physically correct, robust results, we use a spherical orbit modeling method after Schwarzschild (1979), Richstone & Tremaine (1984), and Rix *et al.* (1997) — a fully general way to construct realistic models of a galaxy, given an assumed potential. In §2 we review the observational constraints on the lens galaxies, and introduce constraints on their LOSVD profiles by demonstrating that the profiles of nearby elliptical galaxies are self-similar. We describe our modeling method and demonstrate it with a test-case problem in §3. In §4, we report the range of model solutions for Q0957+561, and discuss the implications for H_0 . We examine the solutions for PG 1115+080 in §5. In §6 we give our conclusions.

2. OBSERVATIONAL CONSTRAINTS

We first review the observational data for Q0957+561 G1 and PG 1115+080 G in §2.1. As discussed in §1, a simple measurement of the central projected stellar velocity dispersion $\hat{\sigma}_p$ cannot strongly constrain the mass of a lens galaxy, necessitating further *a priori* constraints. However, rather than making unjustified assumptions about the galaxy’s anisotropy, we impose conditions on its observable properties by requiring it to have an LOSVD profile consistent with those of better-observed galaxies. To this end, we extract “mean profiles” of $v_{\text{rms}}(R)$ and $h_4(R)$, including their galaxy-to-galaxy scatter, from the observational data available for nearby elliptical galaxies¹. If there proves to be a universal shape to these profiles (*i.e.*, there is little scatter between galaxies), we can use them as additional constraints (see §2.2).

¹As introduced by van der Marel & Franx (1993) and Gerhard (1993), \mathcal{L} is parameterized by the Gauss-Hermite moments,

$$h_l \equiv \sqrt{2} \frac{\gamma_0}{\hat{\gamma}} \int_{-\infty}^{\infty} \mathcal{L}(v_p) e^{-\hat{w}^2/2} H_l(\hat{w}) dv_p, \quad (1)$$

where $\hat{w} = (v_p - \hat{v}_p)/\hat{\sigma}_p$, γ_0 is the line strength, $(\hat{\gamma}, \hat{v}_p, \hat{\sigma}_p)$ are the coefficients for the best Gaussian fit to \mathcal{L} , and $H_l(\hat{w})$ are the Hermite polynomials. A perfectly Gaussian profile will have $h_l = \delta_{0l}$ and $\hat{\sigma}_p = \sigma_p$. For spherical systems, the fourth moment h_4 is a useful constraint on the DF; its value is typically positive (peaked LOSVD) if f is radially anisotropic, and negative (flat-topped LOSVD) if tangentially anisotropic. Strictly speaking, since we apply the data to non-rotating models, we should use the Gauss-Hermite moment z_4 corresponding to the *even* part of the LOSVD (van der Marel *et al.* 1994 §5.1), but such data are not available, and the correction is probably small.

2.1. Observations of Q0957+561 and PG 1115+080

Accurate observations of Q0957+561 G1 are difficult because of the nearby bright quasar image, but measurements have been made of the stellar surface brightness profile $I(R)$ and the central velocity dispersion $\hat{\sigma}_p$. Bernstein, Tyson, & Kochanek (1993) measured $I(a)$ along the major axis ($a = 2''.5\text{--}18''.3$) in the R -band, and Bernstein *et al.* (1997) measured it at smaller radii ($a = 0''.1\text{--}5''.7$) in the V -band. The galaxy is rather round, with an ellipticity increasing with radius ($\epsilon \simeq 0.1, 0.2, 0.4$ for $a \simeq 0''.1, 1''.5, 10''$). We combine the R and V data, assuming a simple offset of 1.34 magnitudes, and map the data to the intermediate radius $m \equiv \sqrt{a(1-\epsilon)}$, resulting in a profile $I(m)$ with $m = 0''.1\text{--}12''.8$, where $R_{\text{eff}} \simeq 4''.5$. To ensure a reasonable $I(m)$ profile, we also impose weak constraints at large and small radii, resulting in 50 data points over the range $m = 0''.0\text{--}29''.4$. Falco *et al.* (1997) measured the central dispersion of G1 to be $\hat{\sigma}_p = 279 \pm 12 \text{ km s}^{-1}$ inside a $0''.6$ ($1.9h^{-1} \text{ kpc}$) radius. Their data suggest a rise in the dispersion at the center, with $\hat{\sigma}_p = 316 \pm 14 \text{ km s}^{-1}$ inside $0''.2$, and $\hat{\sigma}_p = 266 \pm 12 \text{ km s}^{-1}$ outside $0''.2$. Since such a rise is inconsistent with the radial dispersion profiles of nearby galaxies and with the subsequent dispersion measurements of Tonry & Franx (1998), we adopt the total binned measurement of 279 km s^{-1} .

Grogin & Narayan (1996) modeled the lensing properties of Q0957+561, using two different parametric mass models for G1. We will compare our results with their softened power-law sphere (SPLS) model results, where their density profile is $\rho(r) = \rho_0(1 + r^2/r_c^2)^{-\alpha/2}$. Their best-fit parameters are ($\alpha = 1.92^{+0.08}_{-0.09}$, $r_c = 0''.058^{+0''.053}_{-0''.058}$, $\alpha_E = 2''.40^{+0''.28}_{-0''.34}$, at 2σ), where the deflection parameter α_E is related to the central density ρ_0 . This best-fit model is a poor fit to the data (χ^2 per degree of freedom of 6.9), and uses a position for G1 that has been shown to be incorrect (Bernstein *et al.* 1997). But for want of a reanalysis of the lensing constraints, we will adopt this solution in our models.

Impey *et al.* (1998) found that the galaxy PG 1115+080 G is nearly circular, and fit well by a de Vaucouleurs profile with $R_{\text{eff}} = 0''.59 \pm 0''.06$. We approximate the surface brightness of this galaxy by a Hernquist (1990) model with a break radius of $a = 0''.325$ ($R_{\text{eff}} \simeq 0''.59$), modeled as a profile $I(m)$ with 21 bins over the range $m = 0''.0\text{--}2''.1$. Tonry (1998) measured the central dispersion of G to be $\hat{\sigma}_p = 281 \pm 25 \text{ km s}^{-1}$ inside a $0''.6$ ($1.7h^{-1} \text{ kpc}$) radius. Impey *et al.* (1998) fit the lensing constraints with three standard mass models for G: a singular isothermal sphere ($\alpha = 2$, $r_c = 0''$), a modified Hubble profile ($\alpha = 3$, $r_c = 0''.2$), and a constant mass-to-light ratio model. For all the models, the total projected mass inside $R = 1''.15$ was found to be $(1.24\text{--}1.39) \times 10^{11} h^{-1} M_\odot$, depending on the mass model assumed for a nearby galaxy group.

2.2. Self-Similarity of Kinematic Profiles

Bender, Saglia, & Gerhard (1994) measured the LOSVD out to $\sim R_{\text{eff}}$ for a large, “unbiased” sample of galaxies, and derived the profiles $\hat{v}_p(R)$, $\hat{\sigma}_p(R)$, $h_3(R)$, and $h_4(R)$. For our data set, we take from this sample 80 profiles from 28 elliptical galaxies. We find the rms projected velocity \tilde{v}_{rms}

by numerically integrating the positive line profile $\tilde{\mathcal{L}}(v_p)$ with fit parameters $\{\hat{v}_p, \hat{\sigma}_p, h_3, h_4\}$ (see van der Marel & Franx 1993 §2.4). To make a scale-free comparison of the profiles, we renormalize to the central \tilde{v}_{rms} (inside $0.14R_{\text{eff}}$, for direct comparison with the central $\hat{\sigma}_p$ measurement of Q0957+561 G1; or inside $1.1R_{\text{eff}}$ for PG 1115+080 G), and rescale radially by R_{eff} . We use both major and minor axis data, mapping them to the intermediate radius m . We combine the data in radial bins, spaced such that the number of points in each bin is nearly constant ($\simeq 36$). To improve the large-radius constraints, we divide the last bin ($0.7\text{--}1.8 R_{\text{eff}}$) into three bins, with 12–13 points in each bin. As shown in Figure 1b for the case normalized to Q0957+561 G1, the resulting (rescaled) “mean v_{rms} profile” is nearly constant ($\tilde{v}_{\text{rms}} \simeq 0.9 \pm 0.1$ at $1.5R_{\text{eff}}$), while the dispersion $\tilde{\sigma}_p \equiv \langle (v_p - \tilde{v}_p)^2 \rangle^{1/2}$ decreases with radius ($\tilde{\sigma}_p \simeq 0.6 \pm 0.1$ at $1.5R_{\text{eff}}$) due to increasing rotational support in the outer parts of the low-luminosity galaxies (see Davies *et al.* 1983; Fisher, Illingworth, & Franx 1995). We thus find a remarkably universal, flat rms velocity profile inside $1.5R_{\text{eff}}$, for all elliptical galaxies regardless of other properties. Note that v_{rms} is not only less variable than $\hat{\sigma}_p$, but is also a better physical probe of the gravitational potential. The corrections in the mean profiles due to h_3 and h_4 are small, so that $\tilde{\sigma}_p \simeq \hat{\sigma}_p$ to $\sim 0.3\%$ accuracy, and $\tilde{v}_{\text{rms}} \simeq (\hat{v}_p^2 + \hat{\sigma}_p^2)^{1/2}$ to $\sim 5\%$.

To produce the mean h_4 profile, we use the same binning procedure as for v_{rms} (see Figure 1a). We also add data from a sample of six galaxies (Carollo *et al.* 1995; Statler, Smecker-Hane, & Cecil 1996; Gerhard *et al.* 1998) for which h_4 has been measured at larger radii ($1.7\text{--}4.9R_{\text{eff}}$); we combine these points into three additional bins, with $\simeq 12$ points in each bin. Note that these points are not a large sample, and comparisons of different authors’ data sets suggest that the errors in large radius velocity data are generally underestimated. The mean and dispersion range from $h_4 \simeq 0.002 \pm 0.03$ in the central bin to 0.02 ± 0.06 at $1.5R_{\text{eff}}$, and the LOSVD is everywhere consistent with Gaussianity ($h_4 = 0$).

Because our mean profiles are derived from a general data set of elliptical galaxies, they may not accurately represent a brightest cluster galaxy (BCG) like Q0957+561 G1. To gauge the magnitude of any systematic errors thereby caused, we repeat our procedure with 42 velocity profiles from a set of 12 BCGs from Fisher *et al.* (1995), who find that the radial slopes of $\hat{\sigma}_p$ are similar to those of a sample of normal elliptical galaxies. Since their data do not include measurements of h_3 and h_4 , we use the approximations mentioned above for \tilde{v}_{rms} and $\tilde{\sigma}_p$. As shown in Figure 1c, the resulting BCG $\hat{\sigma}_p$ and v_{rms} profiles are consistent to $\sim 5\text{--}10\%$ accuracy with those from the Bender *et al.* (1994) data set, although small-number statistics make the significance of the differences difficult to interpret. We also examine the Bender *et al.* (1994) data for any systematic correlations with other galaxy properties (the absolute magnitude M_B , the dimensionless rotation $[\hat{v}_m / \langle \hat{\sigma}_p \rangle]^*$, and the stellar projected axis ratio q_*). While we find indications that “BCG-like” galaxies have systematically lower h_4 and higher $\tilde{\sigma}_p$ at large radii, they show no clear difference for \tilde{v}_{rms} . Although there are insufficient data available to construct BCG mean profiles, we can still use them to *estimate* the systematic corrections to our modeling results for Q0957+561 G1 (see §4).

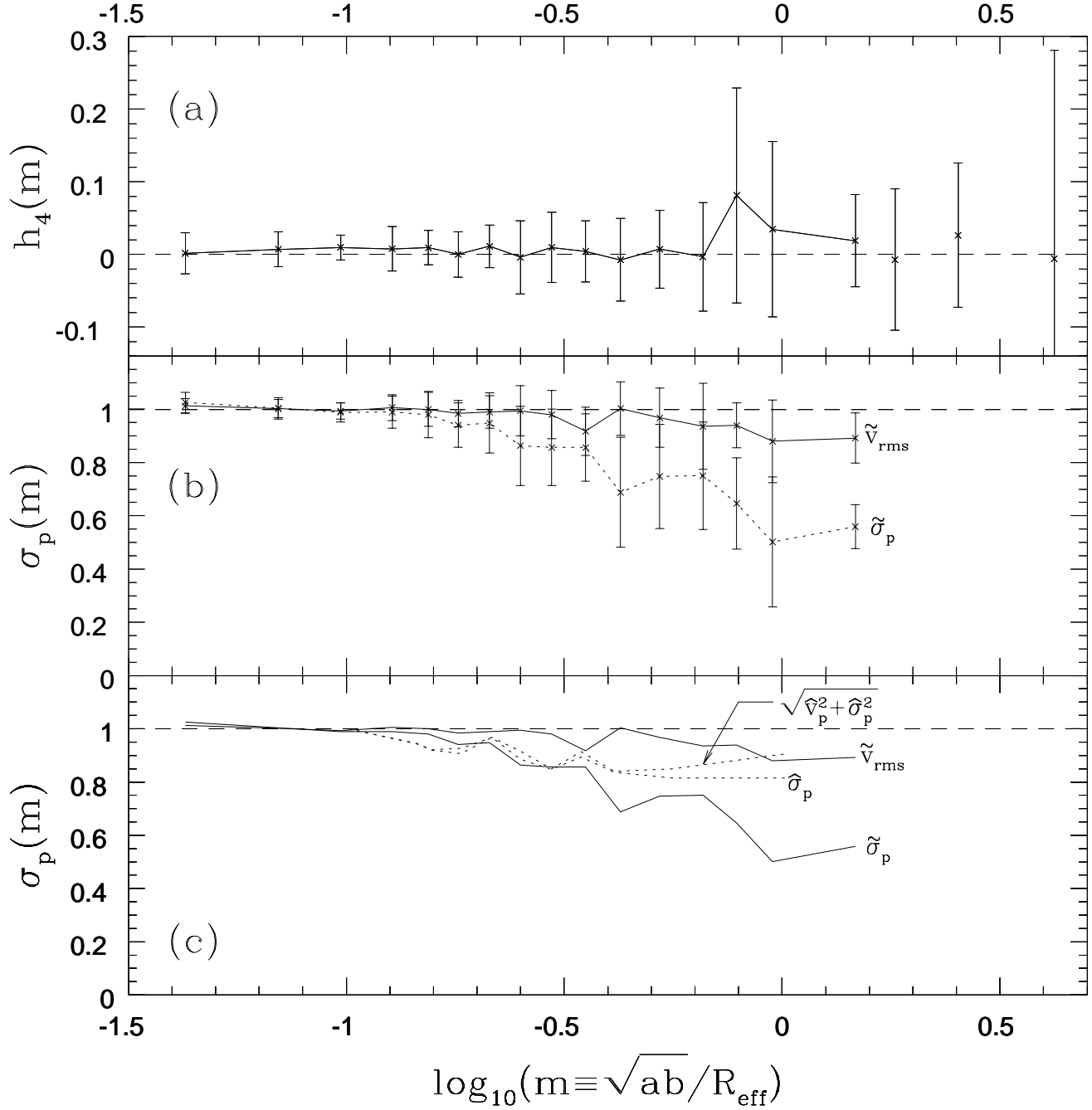


FIG. 1.— Mean profiles computed from elliptical galaxy data. Error bars show the dispersion about the mean. (a) Fourth-order Gauss-Hermite moment. A solid line connects the Bender *et al.* (1994) data. (b) Velocity profiles, from the Bender *et al.* (1994) data, normalized to the total velocity dispersion inside the radius $m = 0.14$. Shown are both the rms velocity (*solid line*) and the velocity dispersion (*dotted line*). (c) Velocity profiles, from the Bender *et al.* (1994) (*solid lines*) and the BCG (*dotted lines*) data. For clarity, the scatter is not shown.

3. METHODS

Schwarzschild (1979) described, and Richstone & Tremaine (1984) extended, a completely general method of dynamical modeling, where a galaxy is built from a library of representative orbits, each weighted with an occupancy number. The weights are adjusted so that the model fits a set of observational constraints — typically the surface brightness and line-of-sight velocities of a galaxy. By construction, the method arrives at a solution that is a physical system of non-negative orbits (thereby avoiding the problems with using the Jeans equations). Unlike other common modeling methods, the method requires explicit knowledge of neither the integrals of motion nor the form of the distribution function. Recent efforts at galaxy modeling have employed sophisticated variants of the method that include fits to higher-order velocity moments (*e.g.*, Rix *et al.* 1997; van der Marel *et al.* 1998).

As discussed in §2.1, we adopt the SPLS family of density profiles for our models, along with the Hernquist (1990) mass model. The initial radii r_{0k} of the orbits are logarithmically spaced in r_0 , and the energy E_k of each orbit is selected to correspond to that of a circular orbit at this radius, $\Phi(r_0) + v_c^2(r_0)/2$. For a singular isothermal potential, the spacing is uniform in energy. The angular momentum L_k of the orbit is selected randomly from the range $[0, L_{\max}]$, where $L_{\max} = r_0 v_c(r_0)$. This procedure ensures dense, uniform coverage of the (E, L) phase space. The model observables \mathbf{y}^m are given by the orbit weights \mathbf{w} and the orbit projection “kernels” \mathbf{K}^m , which are averaged over time and over all spherical-polar viewing angles (θ, ϕ) : $y_i^m = \sum_k w_k^2 \langle K_{ik}^m \rangle_{t, \theta, \phi}$. For example, the kernel for the angle-averaged surface density of an orbit at radius r is given by $\langle K^{I(R)} \rangle_{\theta, \phi} = (2\pi r \sqrt{r^2 - R^2})^{-1}$. The orbit is then run forward in time for one radial period T_r , and the final kernel is found by averaging over time: $\langle K \rangle_{t, \theta, \phi} = T_r^{-1} \int_0^{T_r} \langle K \rangle_{\theta, \phi}(t) dt$. To calculate the Gauss-Hermite velocity moments, we calculate the LOSVD $\mathcal{L}(v_p)$ in 41 velocity bins from $v_p = 0$ to v_{\max} , where the maximum velocity v_{\max} is given by the largest velocity attainable on a radial orbit by the highest-energy orbit. We then perform a nonlinear least-squares fit to find $\hat{\gamma}$ and $\hat{\sigma}_p$, and then use equation (1) to find h_l .

Since the model is typically underconstrained, we fit the model observables \mathbf{y}^m to the data \mathbf{y}^d using the statistic $\chi^2 = \sum_i (y_i^m - y_i^d)^2 / \sigma_i^2$, while optimizing a smoothing function, the entropy $S = \sum_k w_k^2 \ln w_k^2$. This corresponds to minimizing the function $f \equiv \chi^2 + \lambda S$, where the Lagrangian multiplier λ is a smoothing factor. During our modeling runs, we reduce λ slowly from 1 to 10^{-5} to arrive at the limiting case where no smoothing is imposed. Since the velocities scale linearly with the total mass of the galaxy, we can leave the mass dispersion parameter ($\sigma_0^2 \equiv 2\pi G \rho_0 r_c^2$ for the SPLS models) free to vary in the fit. We can also enforce isotropy by minimizing the function $f_i \equiv \sum_i [(\nu v_r^2)_i - (\nu v_t^2)_i]^2 / [(\nu v_r^2)_i + (\nu v_t^2)_i]^2$. We use the conjugate gradient method (Press *et al.* 1992), with first and second derivative information, to minimize f .

We test our methods on a self-consistent (constant mass-to-light ratio) isotropic Hernquist (1990) galaxy, with mass density profile $\rho(r) = M_0 a (2\pi r)^{-1} (r + a)^{-3}$. We fit the exact analytic stellar surface brightness profile $I(R)$ and the projected stellar velocity dispersion profile $\sigma_p(R)$.

Both profiles are measured in 21 annuli from $R = 0$ to $R = 16a$, and are assigned 10% measurement errors. There are 2000 orbits, spaced with initial radii from $0.07a$ to $221a$ ($R_{\text{eff}} \simeq 1.8a$), resulting in a radial coverage from 0 to $442a$. There are a variety of solutions consistent with the data, including the self-consistent isotropic solution. Although the more anisotropic solutions generally show more pronounced deviations from Gaussianity in their LOSVDs, isotropy does not necessarily imply $h_4 = 0$, and vice-versa (see Figure 2).

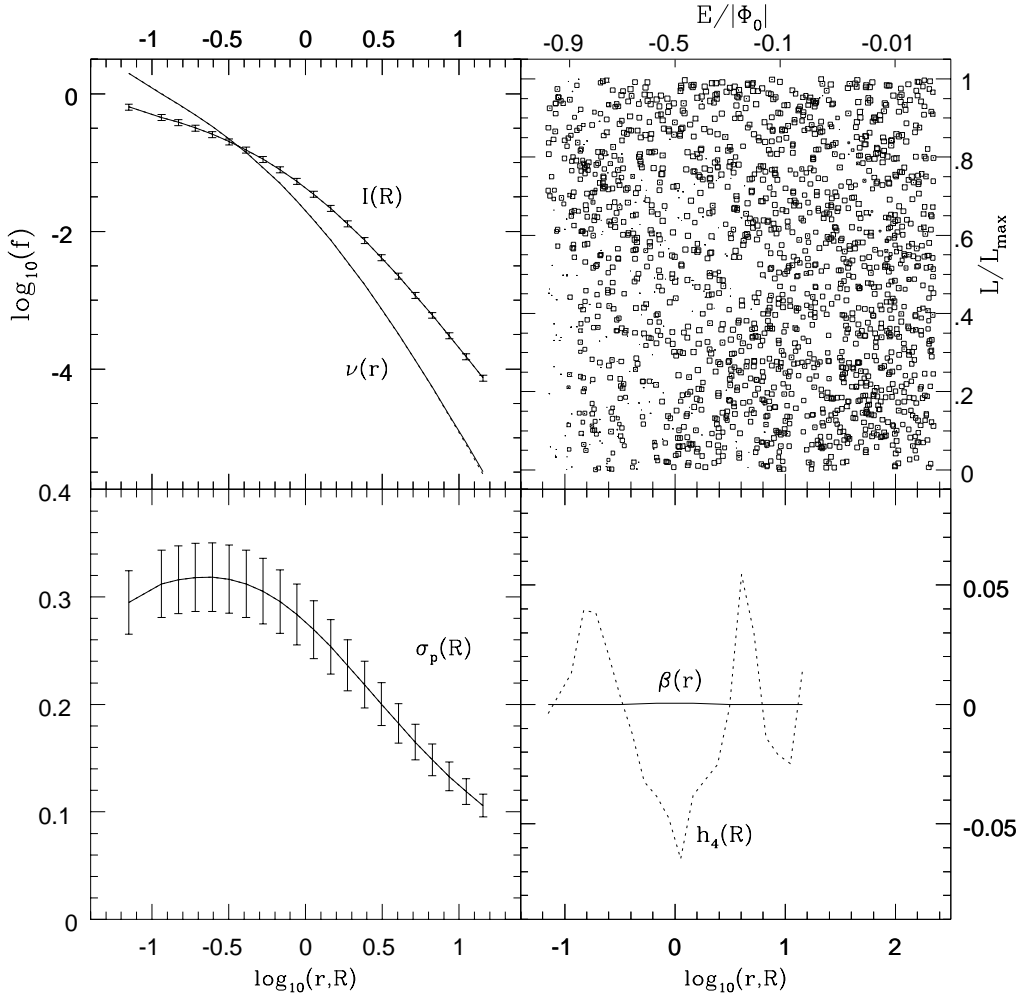


FIG. 2.— Isotropic model solution to simulated Hernquist (1990) galaxy data. *Upper left:* Model (dotted lines) and data (solid lines), for surface brightness (with error bars) and luminosity density. *Lower left:* Same, for projected stellar velocity dispersion. *Upper right:* Orbit weights, in energy-angular momentum phase space. The area of each square is proportional to the logarithm of the orbit's weight. The bottom axis shows the orbit's initial radius, and the top axis its energy. *Lower right:* Anisotropy parameter (solid line) and fourth-order Gauss-Hermite velocity moment (dotted line), as a function of radius. The break radius is $a = 1$ ($R_{\text{eff}} \simeq 1.8$).

4. Q0957+561 RESULTS

We next model the galaxy G1 in Q0957+561, fitting only the measured data: $I(R)$ and central $\hat{\sigma}_p$ (see §2.1). We use the best-fit SPLS mass model from GN, with ($\alpha = 1.92$, $r_c = 0''.058$). There are 2000 orbits with initial radii from $0''.07$ to $221''$, resulting in radial coverage from $0''$ to $361''$. A wide range of solutions fits the data exactly, and we find $1\text{-}\sigma$ limits on the mass dispersion parameter of $\sigma_0 = 295^{+143}_{-121} \text{ km s}^{-1}$, defined by the $\Delta\chi^2 = 1$ boundary about the minimum χ^2 (see Figure 3). Such a large range of possible solutions corresponds to a 73% uncertainty in the mass of G1, but the extreme solutions show radical departures from a constant velocity dispersion profile, and from nearly-Gaussian LOSVDs (see Figure 4). For example, a very massive solution has nearly circular orbits at large radii, so that there are few plunging radial orbits to produce large velocities at the galactic center (see Figure 6). This behavior shows up as a velocity dispersion profile that rises with radius, and has a negative h_4 moment (flat-topped LOSVD) at large radii (see Figure 5).

To reject such solutions, we impose our “mean profile” constraints on $\hat{\sigma}_p(R)$ and $h_4(R)$ (see §2.2; note that the spherical symmetry in our model implies $v_{\text{rms}} \simeq \hat{\sigma}_p$). We find that the range of viable solutions is dramatically reduced (Fig. 3), with new $1\text{-}\sigma$ limits on σ_0 of $280^{+19}_{-26} \text{ km s}^{-1}$, and $2\text{-}\sigma$ limits of $280^{+29}_{-34} \text{ km s}^{-1}$. Some of these solutions may not be dynamically stable, but incorporating stability criteria into our model fitting is beyond the scope of this project.

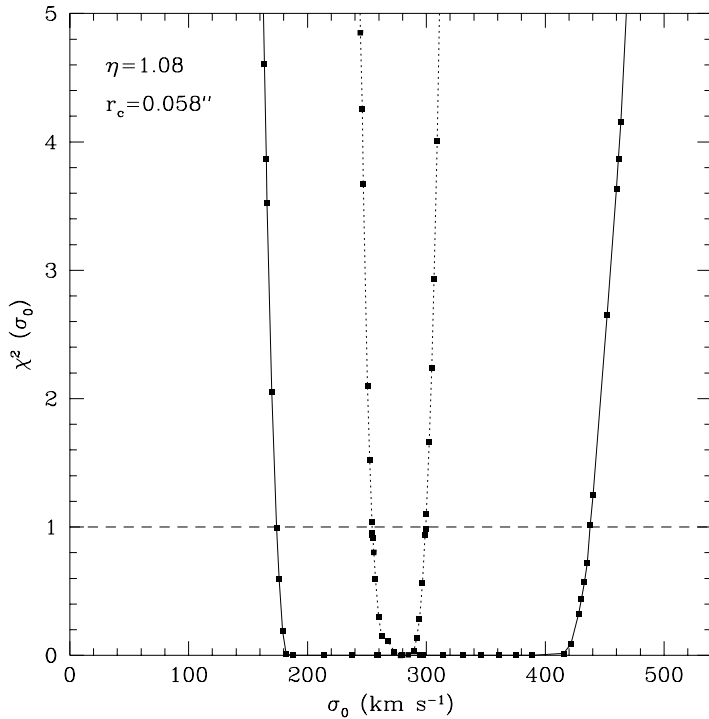


FIG. 3.— Chi-square of the best-fit lens mass model to the Q0957+561 G1 data (surface brightness and central projected velocity dispersion), as a function of the mass dispersion (*solid line*). Also shown are the fits including the mean $\hat{\sigma}_p(R)$ and $h_4(R)$ constraints (*dotted line*).

Since the reduced range of the solutions depends on the application of our mean profile constraints, we next investigate the sensitivity of the results to our main concerns about these constraints. First, we remove the constraints on h_4 at large radii ($R > 1.8R_{\text{eff}}$), where the reliability of the local galaxy data is questionable. This increases the best-fit σ_0 and its uncertainty by less than 1 km s^{-1} . Second, we estimate the effect of a systematic bias. Since we found in §2.2 that BCGs may have systematically lower h_4 at large radii, we examine an extreme case where we set $h_4 = -0.06$ for $R > 1''.2$. We find new $1\text{-}\sigma$ limits of $\sigma_0 = 287^{+15}_{-18} \text{ km s}^{-1}$, indicating that the systematic correction for galaxy type would increase σ_0^2 (and H_0) by at most 5%. In summary, we find $1\text{-}\sigma$ limits on σ_0 of $280^{+19}_{-26} \text{ km s}^{-1}$, which corresponds to a 16% uncertainty in the mass of G1. Part of the uncertainty in σ_0 is due to the measurement error of the central $\hat{\sigma}_p$ (12 km s^{-1}), while part is due to the systematic uncertainty in converting from $\hat{\sigma}_p$ to σ_0 ($\sim 19 \text{ km s}^{-1}$). This contrasts strongly with the conversion from GN, which implies (by assuming the anisotropy $\beta(r)$ to be constant and near zero) $1\text{-}\sigma$ limits of $\sigma_0 = 290^{+12}_{-13} \text{ km s}^{-1}$. Their reported systematic uncertainty of 2 km s^{-1} is clearly underestimated, given that our best dynamical model is systematically different from theirs by a factor five times larger.

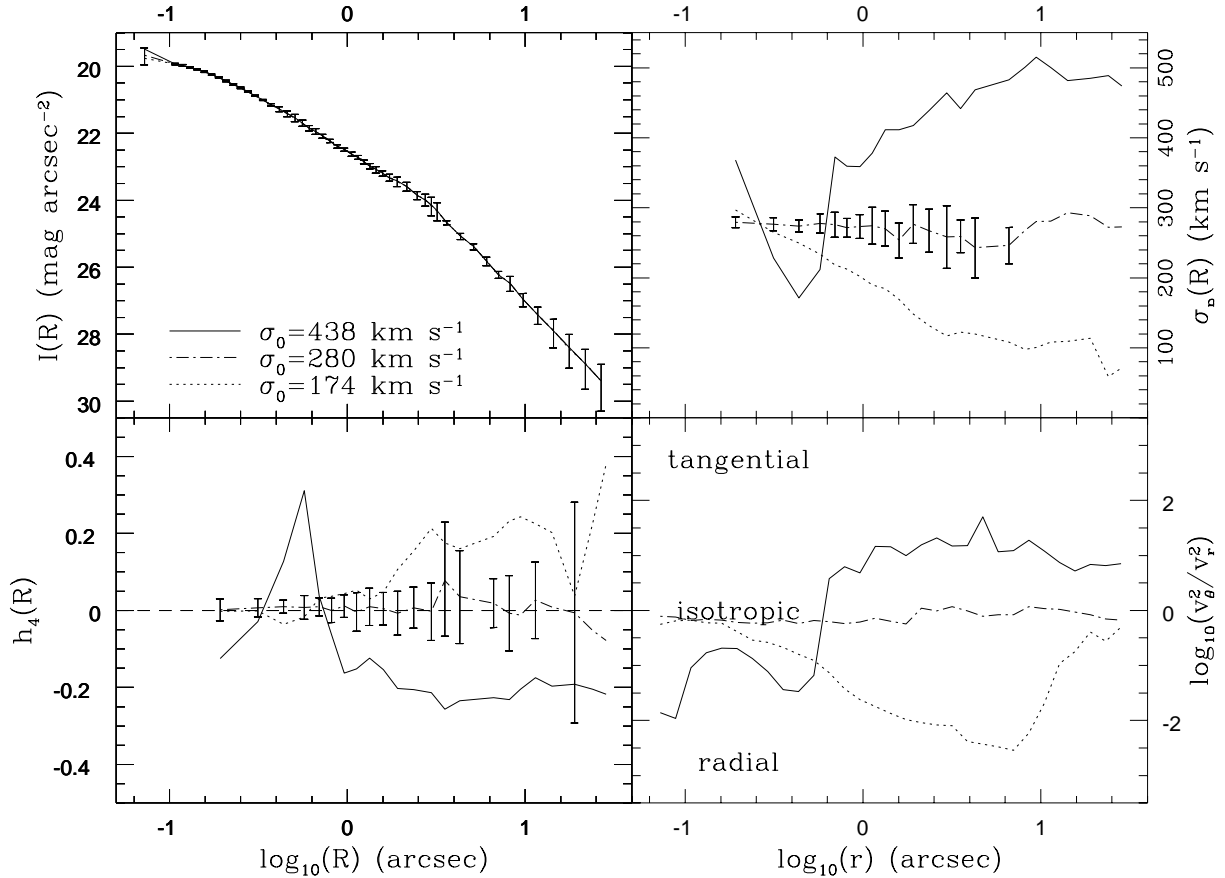


FIG. 4.— Solutions for Q0957+561 G1, for several mass dispersions. The solutions are all acceptable ($\Delta\chi^2 < 1$), given only the surface brightness and central velocity dispersion data. *Upper left:* Surface brightness profile, where the error bars show data from Bernstein *et al.* (1993, 1997). *Lower left:* Fourth-order Gauss-Hermite moment profile, with the “mean profile” shown by error bars (see §2.2). *Upper right:* Velocity dispersion profile, with the mean profile shown by error bars. *Lower right:* Anisotropy profile.

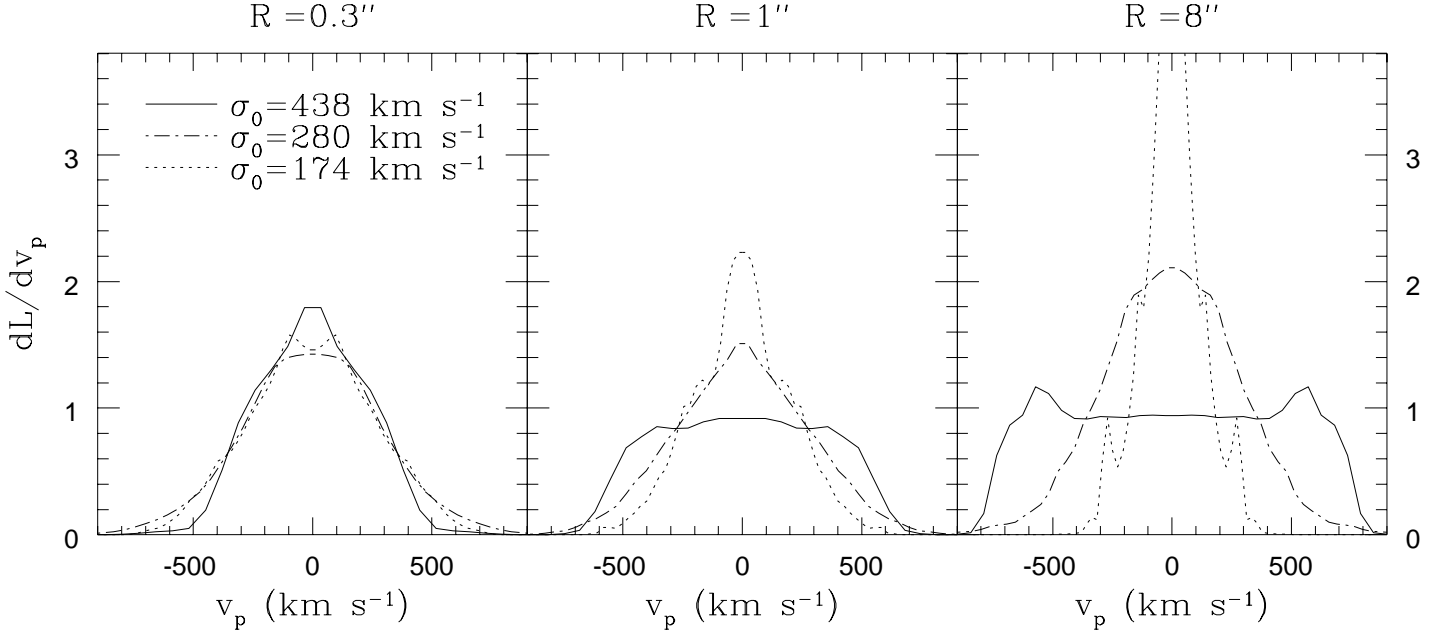


FIG. 5.— Line-of-sight velocity distributions, for the same solutions, at several radii.

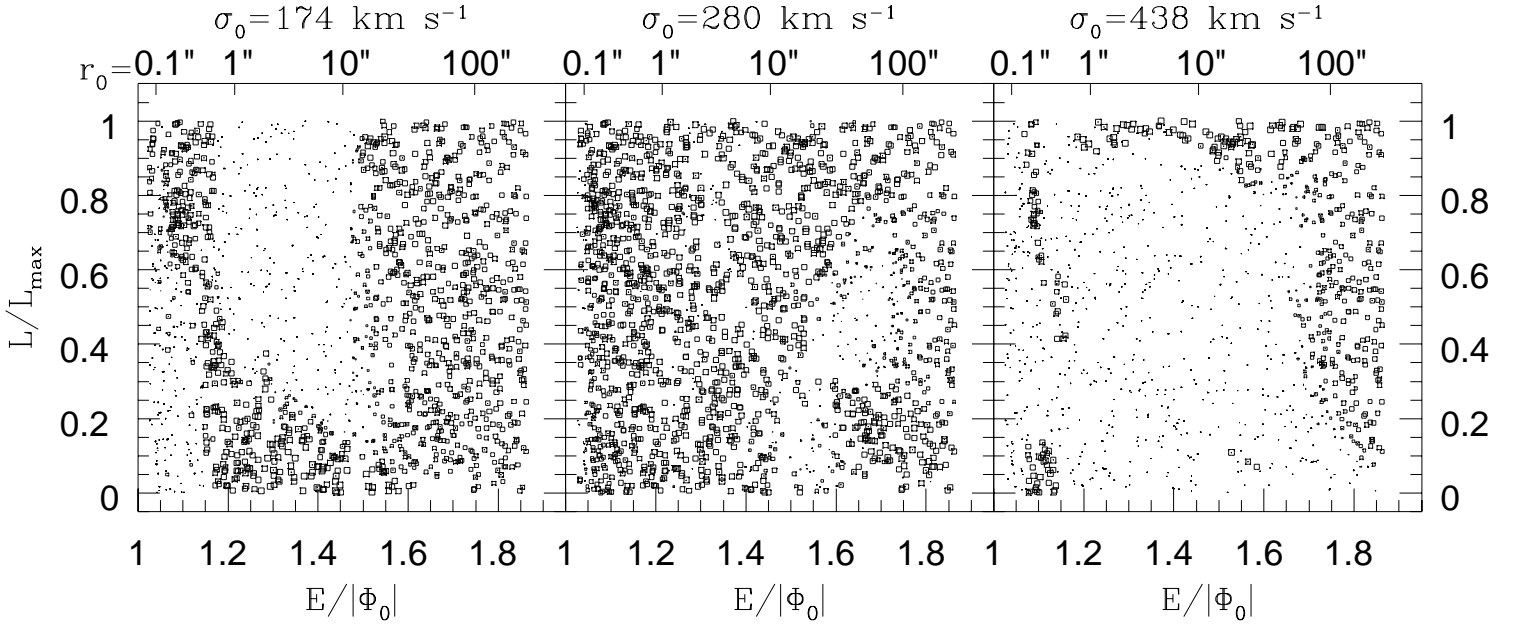


FIG. 6.— Orbit weights for the same solutions, plotted in energy-angular momentum phase space. The area of each square is proportional to the logarithm of the orbit's weight. The top axis shows the initial radius.

We next compare our results with the Q0957+561 lens models of GN to produce new bounds on the Hubble constant H_0 . Given their best fit mass model ($\alpha = 1.92, r_c = 0''.058$), GN found 1- σ limits on the deflection parameter α_E of $2''.40 \pm 0''.07$. As mentioned in §1, the conversion of α_E to the G1 mass dispersion σ_0 is subject to a well-known degeneracy between the galaxy mass and the cluster mass: one can add a cluster with a convergence κ , and decrease the galaxy mass by the factor $(1 - \kappa)$. Since this degeneracy affects none of the image observables but the time delay, H_0 is systematically uncertain by the same factor $(1 - \kappa)$. Thus, with the time delay measurement of Kundić *et al.* (1997), and density parameter $\Omega_0 = 1$, the GN results imply $\sigma_0 = (324 \pm 4)\sqrt{1 - \kappa}$ km s⁻¹ and $H_0 = (82 \pm 2)(1 - \kappa)$ km s⁻¹ Mpc⁻¹. Our dynamical constraints on σ_0 therefore put 1- σ constraints on κ of $0.25^{+0.14}_{-0.10}$, implying $H_0 = 61^{+9}_{-11}$ km s⁻¹ Mpc⁻¹; and 2- σ constraints of $\kappa = 0.25^{+0.19}_{-0.16}$, implying $H_0 = 61^{+13}_{-15}$ km s⁻¹ Mpc⁻¹ (see Figure 7). Note that Tonry & Franx (1998) measured a central velocity dispersion for G1 of $\hat{\sigma}_p = 288 \pm 9$ km s⁻¹; although their aperture is different from that used in our dynamical models, their measurement would roughly imply $\kappa \simeq 0.20 \pm 0.12$ and $H_0 \simeq 65 \pm 10$ km s⁻¹ Mpc⁻¹.

For comparison, we examine complementary studies of this system. Fischer *et al.* (1997) used the weak lensing of background galaxies to determine the surface density $\Sigma(R)$ of the cluster. Using their parameterized model fit to Σ and their stated uncertainties, we find 1- σ constraints on the convergence κ of $0.19^{+0.33}_{-0.09}$, and 2- σ bounds of (0.06-1.00). Similarly, Kundić *et al.* (1997) estimated $\kappa = 0.22 \pm 0.14$ (2 σ) from this data, but they neglected the uncertainties in the cluster position. Note that these estimates of κ were derived with the cluster centered on the galaxy G1, rather than at the real mass centroid of the cluster, and also that the proximity of the cluster to G1 invalidates the description of the potential as simply a convergence κ and a shear γ (see Kochanek 1991). Kundić *et al.* (1997) also warn that an error in the assumed mean redshift of the background galaxies can affect the derived H_0 significantly. With these *caveats* in mind, we find that the 1- σ values for κ from the Fischer *et al.* (1997) models imply $\sigma_0 = 291^{+16}_{-59}$ km s⁻¹ for the best-fit GN model, and $H_0 = 66^{+8}_{-27}$ km s⁻¹ Mpc⁻¹ (see Fig. 7). In a complementary study, Chartas *et al.* (1998) determined the mass of the cluster from its gaseous X-ray emission. Their results imply $\kappa = 0.11 \pm 0.04$, $\sigma_0 = 306 \pm 17$ km s⁻¹, and $H_0 = 73 \pm 6$ km s⁻¹ Mpc⁻¹ (2 σ), but they include no estimate of their systematic uncertainties.

Both of these direct constraints on κ are consistent with the constraints implied by our dynamical models of G1, and could in principle be combined with them to further constrain H_0 , though they are currently too uncertain to add any useful information. So we find that the GN lens model, combined with the dispersion measurement of G1, permits a determination of H_0 to 16% accuracy. Although better lens models may significantly shift the best-fit H_0 value, they will have little effect on the uncertainties, which are dominated by the uncertainty in κ ; we have already assumed a perfect determination of the parameters (α, r_c) from the GN models, and a perfect determination of α_E would tighten the 1- σ limits on H_0 by only ~ 0.1 km s⁻¹ Mpc⁻¹. To find H_0 to significantly better accuracy from this system, we would need much better direct constraints on the cluster mass distribution, and/or highly accurate velocity data from the galaxy at larger radii.

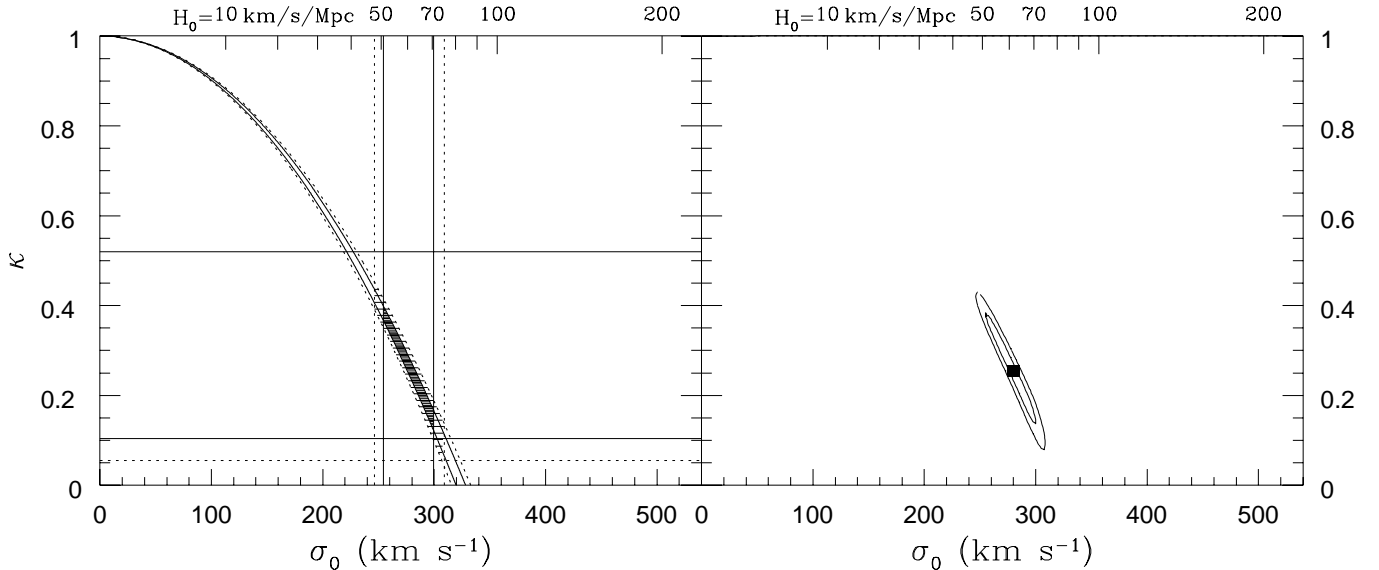


FIG. 7.— Constraints on galaxy mass dispersion σ_0 , cluster convergence κ , and Hubble constant H_0 . The left panel shows a diagram of the independent constraints. The solid lines show 1- σ bounds on σ_0 and κ , and the dotted lines show 2- σ bounds. The curved lines show the constraints on σ_0 and κ from the GN lens models. The horizontal lines show the constraints on κ from Fischer *et al.* (1997). The vertical lines show our constraints on σ_0 . The approximate region of parameter space permitted at the 1- σ level is indicated by dark shading; the 2- σ region by light shading. The right panel shows a contour plot of the permitted region (including the GN and σ_0 constraints), with 1- σ and 2- σ bounds. The point marks the best-fit solution.

5. PG1115+080 RESULTS

We next model the galaxy G in PG 1115+080 to determine if the different lens mass profiles explored by Impey *et al.* (1998) are consistent with the measurements by Impey *et al.* (1998) of $I(R)$ and by Tonry (1998) of the central $\hat{\sigma}_p$ (see §2.1). If any mass model can be ruled out, so can its corresponding value of H_0 . As in the case of Q0957+561, a single central $\hat{\sigma}_p$ measurement will give us little information about the galaxy mass profile, so we again impose mean profile constraints on $v_{\text{rms}}(R)$ and $h_4(R)$, normalized to this galaxy (see §2.2).

We fit a singular isothermal mass model to these data, and although we have not exhaustively explored the entire range of possible solutions, we estimate the projected mass inside $R = 1''.15$ to be $M = 1.7^{+0.3}_{-0.7} \times 10^{11} h^{-1} M_\odot$, which is consistent with the lens model's implied $M = (1.25 \pm 0.02) \times 10^{11} h^{-1} M_\odot$ (for the case where the nearby galaxy group is modeled as a singular isothermal sphere). Similarly, we fit the modified Hubble model and find $M = (1.6 \pm 0.5) \times 10^{11} h^{-1} M_\odot$, which is consistent with the lens model fit mass. To test the constant mass-to-light ratio hypothesis, we fit a Hernquist (1990) model with a break radius of $a = 0''.325$ (to match the measured effective radius of $R_{\text{eff}} = 0''.59$), and find $M = 1.3^{+0.3}_{-0.4} \times 10^{11} h^{-1} M_\odot$, which is also consistent with the lens

model fit mass. Our dynamical models are also consistent with the lens model results when the group is modeled as a point mass, in which case $M \simeq 1.4 \times 10^{11} h^{-1} M_{\odot}$. To compare the relative likelihood of the three mass models, we impose the lens model mass normalization on each of them, and find that our dynamical solutions are statistically indistinguishable ($\Delta\chi^2 < 1$).

With the measured time delay (Schechter *et al.* 1997 ; Barkana 1997b), for $\Omega_0 = 1$ and a singular isothermal group model, the singular isothermal galaxy model gives $H_0 = 44 \pm 4 \text{ km s}^{-1} \text{ Mpc}^{-1}$; the modified Hubble profile model, $61 \pm 5 \text{ km s}^{-1} \text{ Mpc}^{-1}$; and the constant M/L model, $65 \pm 5 \text{ km s}^{-1} \text{ Mpc}^{-1}$ (Impey *et al.* 1998). Treating the group as a point mass increases H_0 by $\sim 10\%$. Since our stellar dynamical models do not rule out any of the lens models, a large range of values for H_0 is still permitted by the system. As in the case of Q0957+561, stronger constraints on the mass distribution of the system (e.g., from LOSVD measurements of the lens galaxy, or from more detailed observations of the Einstein ring) will be necessary to break the model degeneracies.

6. CONCLUSIONS

Using very general orbit modeling methods, we have examined the uncertainty in the mass of the lens galaxies Q0957+561 G1 and PG 1115+080 G, given observations of their central projected stellar velocity dispersions $\hat{\sigma}_p$ (Falco *et al.* 1997; Tonry 1998). As many past studies have shown, such a measurement alone is inadequate to strongly constrain the galaxy’s mass. In order to put additional realistic *a priori* constraints on the galaxy’s properties, we have derived “mean profiles” of the rms projected velocity $v_{\text{rms}}(R)$ and the fourth-order Gauss-Hermite moment $h_4(R)$ from a large sample of nearby elliptical galaxies. These mean profiles prove to be remarkably self-similar, even over a large range of galaxy types. This universality is not too surprising, given the homology of early-type galaxies implied by the existence of the fundamental plane — an even stronger implication if the central kinetic energy is considered instead of the velocity dispersion (e.g., Busarello *et al.* 1997).

For Q0957+561 G1, given the best-fit SPLS mass model from Grogin & Narayan (1996), with only the surface brightness profile $I(R)$ and central $\hat{\sigma}_p$ as constraints, we find 1- σ limits on the mass dispersion σ_0 of $295^{+143}_{-121} \text{ km s}^{-1}$. The addition of the mean profile constraints reduces this permitted range to $280^{+19}_{-26} \text{ km s}^{-1}$. In conjunction with the GN lens model constraints, this implies a cluster convergence of $\kappa = 0.25^{+0.14}_{-0.10}$, which is consistent with the constraints on κ from other independent studies. Using the time delay measurement of Kundić *et al.* (1997), we find 1- σ limits on H_0 of $61^{+9}_{-11} \text{ km s}^{-1} \text{ Mpc}^{-1}$, and 2- σ limits of $61^{+13}_{-15} \text{ km s}^{-1} \text{ Mpc}^{-1}$. *Thus, current measurements of the lens system Q0957+561 do not constrain H_0 to better than 15%.* To obtain useful limits on H_0 , we will need better constraints on the cluster convergence and/or better velocity profile measurements for the galaxy G1. We will also need substantial revision of the lens model — the GN solutions fit the lens data poorly, inaccurately assume a spherical galaxy, and use an oversimplified Taylor expansion model of the cluster. Presumably a more accurate lens model will eventually provide a good fit to the data and a different value for H_0 (see Barkana *et al.* 1998 for some improved

models), in which case our dynamical model will still be illustrative of the systematic uncertainties expected.

We have also examined the lens galaxy PG 1115+080 G, which has a total mass that is relatively well-determined by the lensing constraints, but a radial mass distribution that is unconstrained (Impey *et al.* 1998). As with Q0957+561 G1, we model this galaxy by including constraints on $I(R)$ and the central $\hat{\sigma}_p$ along with the mean profile constraints. We find that these constraints are not sufficient to break the degeneracy between the different lens models, so that a large range of values is still permitted for H_0 (44-68 km s⁻¹ Mpc⁻¹). Further constraints on the mass distribution in this system are needed.

The stellar dynamics of gravitational lens systems show considerable promise for determining H_0 , even if we have only central dispersions. Larger samples of dispersion measurements would be particularly valuable, since each lens system will have a different set of systematic uncertainties (it is encouraging to note that the results for H_0 from Q0957+561 and PG 1115+080 are so far consistent with each other). Of particular value would be results from isolated systems with lens geometries that probe the radial mass distribution, such as MG 1654+1346 (see Ellithorpe, Kochanek, & Hewitt 1996) and MG 1549+3047 (Lehár *et al.* 1993, 1996). The results from a large set of these systems could be combined using Bayesian methods to converge on a robust value for H_0 (see Press 1997), avoiding the correlated systematic uncertainties that plague “distance ladder” approaches. Furthermore, the independent measurement of galaxy properties from gravitational lensing and from stellar dynamics has an enormous potential for shedding light on the detailed structure of galaxies.

We thank Ralf Bender and Roberto Saglia for providing their data in tabular form; Marijn Franx, Ramesh Narayan, John Tonry, and the anonymous referee for helpful comments; and Roeland van der Marel for both. We also thank Norm Grogin for many further demonstrations of his lens models. C.S.K. is supported by NSF grant AST 94-01722 and NASA ATP grant NAG 5-4062.

REFERENCES

- Angonin-Willaime, M.-C., Soucail, G., & Vanderriest, C. 1994, *A&A*, 291, 411
- Bar-Kana, R. 1997a, Ph.D. thesis, Massachusetts Institute of Technology
- Barkana, R. 1997b, *ApJ*, 489, 21
- Barkana, R., Lehár, J., Falco, E. E., Grogin, N. A., Keeton, C. R., & Shapiro, I. I. 1998, *ApJ*, [astro-ph/9808096](#)
- Bender, R., Saglia, R. P., & Gerhard, O. E. 1994, *MNRAS*, 269, 785
- Bernstein, G., Fischer, P., Tyson, J. A., & Rhee, G. 1997, *ApJ*, 483, L79
- Bernstein, G. M., Tyson, J. A., & Kochanek, C. S. 1993, *AJ*, 105, 816
- Binney, J., & Mamon, G. A. 1982, *MNRAS*, 200, 361
- Busarello, G., Capaccioli, M., Capozziello, S., Longo, G., & Puddu, E. 1997, *A&A*, 320, 415
- Carollo, C. M., de Zeeuw, P. T., van der Marel, R. P., Danziger, I. J., & Qian, E. E. 1995, *ApJ*, 441, L25
- Chartas, G., Falco, E., Forman, W., Jones, C., Schild, R., & Shapiro, I. 1995, *ApJ*, 445, 140
- Chartas, G., Chuss, D., Forman, W., Jones, C., & Shapiro, I. 1998, *ApJ*, 504, 661
- Courbin, F., Magain, P., Keeton, C. R., Kochanek, C. S., Vanderriest, C., Jaunsen, A. O., & Hjorth, J. 1997, *A&A*, 324, L1
- Dahle, H., Maddox, S. J., & Lilje, P. B. 1994, *ApJ*, 435, L79
- Davies, R. L., Efstathiou, G., Fall, S. M., Illingworth, G., & Schechter, P. L. 1983, *ApJ*, 266, 41
- Dejonghe, H. 1987, *MNRAS*, 224, 13
- Dejonghe, H., & Merritt, D. 1992, *ApJ*, 391, 531
- Ellithorpe, J. D., Kochanek, C. S., & Hewitt, J. N. 1996, *ApJ*, 464, 556
- Falco, E. E., Gorenstein, M. V., & Shapiro, I. I. 1985, *ApJ*, 289, L1
- Falco, E. E., Shapiro, I. I., Moustakas, L. A., & Davis, M. 1997, *ApJ*, 484, 70
- Fischer, P., Bernstein, G., Rhee, G., & Tyson, J. A. 1997, *AJ*, 113, 521
- Fisher, D., Illingworth, G., & Franx, M. 1995, *ApJ*, 438, 539
- Garrett, M. A., Walsh, D., & Carswell, R. F. 1992, *MNRAS*, 254, 27P
- Gerhard, O. E. 1991, *MNRAS*, 250, 812
- Gerhard, O. E. 1993, *MNRAS*, 265, 213
- Gerhard, O., Jeske, G., Saglia, R. P., & Bender, R. 1998, *MNRAS*, 295, 197
- Gorenstein, M. V., Falco, E. E., & Shapiro, I. I. 1988, *ApJ*, 327, 693
- Grogin, N. A., & Narayan, R. 1996, *ApJ*, 464, 92 (erratum 473, 570) (GN)

- Haarsma, D. B., Hewitt, J. N., Lehár, J., & Burke, B. F. 1997, *ApJ*, 479, 102
- Haarsma, D. B., Hewitt, J. N., Lehár, J., & Burke, B. F. 1998, *ApJ*, *astro-ph/9807115*
- Hernquist, L. 1990, *ApJ*, 356, 359
- Impey, C. D., Falco, E. E., Kochanek, C. S., Lehár, J., McLeod, B. A., Rix, H.-W., Peng, C. Y., & Keeton, C. R. 1998, *astro-ph/9803207*
- Katz, N., & Richstone, D. O. 1985, *ApJ*, 296, 331
- Keeton, C. R., & Kochanek, C. S. 1997, *ApJ*, 487, 42
- Kochanek, C. S. 1991, *ApJ*, 382, 58
- Kochanek, C. S. 1993, *ApJ*, 419, 12
- Kochanek, C. S. 1994, *ApJ*, 436, 56
- Kundić, T., *et al.* 1997, *ApJ*, 482, 75
- Lehár, J., Langston, G. I., Silber, A., Lawrence, C. R., & Burke, B. F. 1993, *AJ*, 105, 847
- Lehár, J., Cooke, A. J., Lawrence, C. R., Silber, A. D., & Langston, G. I. 1996, *AJ*, 111, 1812
- van der Marel, R. P., & Franx, M. 1993, *ApJ*, 407, 525
- van der Marel, R. P., Evans, N. W., Rix, H.-W., White, S. D. M., & de Zeeuw, T. 1994, *MNRAS*, 271, 99
- van der Marel, R. P., Cretton, N., de Zeeuw, P. T., & Rix, H.-W. 1998, *ApJ*, 493, 613
- Merrifield, M. R., & Kent, S. M. 1990, *AJ*, 99, 1548
- Merritt, D. 1987, *ApJ*, 313, 121
- Merritt, D. 1993, *ApJ*, 413, 79
- Merritt, D., & Saha, P. 1993, *ApJ*, 409, 75
- Plummer, H. C. 1991, *MNRAS*, 71, 460
- Press, W. H., Teukolsky, S. A., Vetterling, W. T., & Flannery, B. P. 1992, *Numerical Recipes in C*, 2nd edn. (Cambridge: Cambridge Univ. Press)
- Press, W. H. 1997, in *Unsolved Problems in Astrophysics*, ed. J. N. Bahcall & J. P. Ostriker (Princeton: Princeton Univ. Press), 49
- Rhee, G. 1991, *Nature*, 350, 211
- Richstone, D. O., & Tremaine, S. 1984, *ApJ*, 286, 27
- Rix, H.-W., & White, S. D. M. 1992, *MNRAS*, 254, 389
- Rix, H.-W., de Zeeuw, P. T., Cretton, N., van der Marel, R. P., & Carollo, C. M. 1997, *ApJ*, 488, 702
- Saha, P., & Williams, L. L. R. 1997, *MNRAS*, 292, 148
- Schechter, P. L., *et al.* 1997, *ApJ*, 475, L85

- Schild, R., & Thomson, D. J. 1997, *AJ*, 113, 130
- Schwarzschild, M. 1979, *ApJ*, 232, 236
- Statler, T. S., Smecker-Hane, T., & Cecil, G. N. 1996, *AJ*, 111, 1512
- Tonry, J. L. 1983, *ApJ*, 266, 58
- Tonry, J. L. 1998, *AJ*, 115, 1
- Tonry, J. L., & Franx, M. 1998, *ApJ*, [astro-ph/9809064](#)
- Walsh, D., Carswell, R. F., & Weymann, R. J. 1979, *Nature*, 279, 381
- Weymann, R. J., Latham, D., Angel, J. R. P., Green, R. F., Liebert, J. W., Turnshek, D. A.,
Turnshek, D. E., & Tyson, J. A. 1980, *Nature*, 285, 641
- Zhao, H., & Prada, F. 1996, *MNRAS*, 282, 1223